HHS Public Access

Author manuscript

Chemistry. Author manuscript; available in PMC 2016 December 07.

Published in final edited form as:

Chemistry. 2015 December 7; 21(50): 18047–18051. doi:10.1002/chem.201504087.

Enzymatic Dissolution of Biocomposite Solids Consisting of Phosphopeptides to Form Supramolecular Hydrogels

Mr Junfeng Shi,
Department of Chemistry, Brandeis University, 415 South St, Waltham, MA 02454, USA, Fax: (+) 1-781-736-2516

Ms. Dan Yuan,
Department of Chemistry, Brandeis University, 415 South St, Waltham, MA 02454, USA, Fax: (+) 1-781-736-2516

Mr. Richard Haburcak,
Department of Chemistry, Brandeis University, 415 South St, Waltham, MA 02454, USA, Fax: (+) 1-781-736-2516

Mr. Qiang Zhang,
Nano-fabrication, Imaging & Characterization Core Lab, King Abdullah University of Science and Technology, Thuwal 23955-6900, Saudi Arabia

Dr. Chao Zhao,
Nano-fabrication, Imaging & Characterization Core Lab, King Abdullah University of Science and Technology, Thuwal 23955-6900, Saudi Arabia

Prof. Xixiang Zhang, and
Nano-fabrication, Imaging & Characterization Core Lab, King Abdullah University of Science and Technology, Thuwal 23955-6900, Saudi Arabia

Prof. Dr. Bing Xu
Department of Chemistry, Brandeis University, 415 South St, Waltham, MA 02454, USA, Fax: (+) 1-781-736-2516

Bing Xu: bxu@brandeis.edu

Abstract

Enzyme-catalyzed dephosphorylation is essential for biomineralization and bone metabolism. Here we report the exploration of using enzymatic reaction to transform biocomposites of phosphopeptides and calcium (or strontium) ions to supramolecular hydrogels as a mimic of enzymatic dissolution of biominerals. ^{31}P NMR shows that strong affinity between the phosphopeptides and alkaline metal ions (e.g., Ca^{2+} or Sr^{2+}) induces the formation of biocomposites as precipitates. Electron microscopy reveals that the enzymatic reaction regulates the morphological transition from particles to nanofibers. Rheology confirms the formation of a rigid hydrogel. As the first example of enzyme-instructed dissolution of a solid to form

Correspondence to: Bing Xu, bxu@brandeis.edu.

Supporting information for this article is available on the WWW under http://www.angewandte.org or from the author.

supramolecular nanofibers/hydrogels, this work provides an approach to generate soft materials with desired properties, expands the application of supramolecular hydrogelators, and offers insights to control the demineralization of calcified soft tissues.

Graphical Abstract

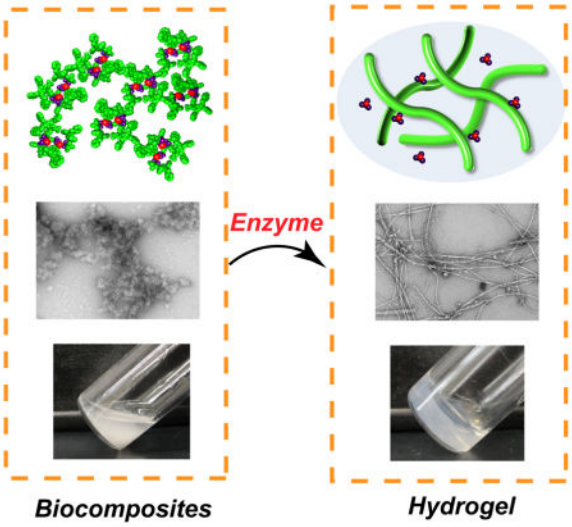

Keywords

phosphopeptide; solid-gel transition; enzyme; self-assembly; bone mineralization

This communication reports the use of enzyme to convert solids to hydrogels. It is known that enzyme-catalyzed dephosphorylation is essential for hydroxyapatite mineralization in bone,[1] an important morphological transformation in biology. Tissue nonspecific alkaline phosphatase (TNAP) hydrolyzes inorganic pyrophosphate to release phosphate, which binds with calcium to initiate and propagate the formation of hydroxyapatite crystal.[2] Thus the deficiency of alkaline phosphatase results in hypophosphatasia, exhibited as poorly mineralized bone.[3] Therefore, the use of enzymatic reaction to kinetically regulate the metabolism of bone in the context of extracellular matrices (ECM) could contribute for understanding bone diseases. Meanwhile, supramolecular hydrogels, driven by self-assembly of small molecules to form three-dimensional networks in water, has received increasing attention [4] because they exhibit considerable physical and mechanical resemblance to the ECM in human tissues. Based on the biological relevance of enzymes, we and others have been developing enzyme-instructed self-assembly and supramolecular hydrogelation.[5] Notably, almost all of the reported hydrogelation starts from a homogeneous solution state and is the result of sol-gel transition, with several exceptions that show the transition of homotypic suspensions of peptides to hydrogels.[6] Though few efforts have focused on solid-gel transitions, solid-to-gel transitions occur in nature. For example, in pycnodysostosis,[7] osteoclast cells destroy only the apatite crystals, but maintain the extracellular matrix of bones. Such a process essentially acts as a form of solid-gel transition. Particularly, Smith et al. pioneered the use of a proteinase enzyme to

effectively remove the nucleus pulposus, which provides a novel approach to restore calcified soft tissues.[8] More importantly, dynamic control of supramolecular self-assembly is emerging as a new model system for mimicking biological transformations.[9] Inspired by the above fundamental advances, we design a phosphopeptide that binds alkaline earth metal ions (e.g., Ca^{2+} and Sr^{2+}) to form biocomposite precipitates, which transform to a supramolecular hydrogel in the presence of an enzyme (i.e., alkaline phosphatase).

Scheme 1 illustrates the concept of enzyme-instructed solid-gel transition. A phosphopeptide (**1P**) interacts with calcium (or strontium) cations to form precipitated biocomposites, which are in equilibrium between dissolved and precipitated states. Upon the addition of the enzyme, the phosphopeptide turns into a hydrogelator (**1**), which self-assembles to form supramolecular nanofibrils constituting the matrices of a hydrogel. The metal cations, after dissociating from the phosphopeptides, re-deposit as calcium (or strontium) phosphates on the surface of the nanofibers of **1** when the calcium (or strontium) phosphate is saturated. Residing in a solid state, a solution phase, and a gel phase, the metal ions participate in dynamic phase transitions that parallel bone metabolism, a fundamental and biological transition that interconverts hard and soft materials. Our results not only confirm that the amount of the enzyme plays a key role in the kinetics of solid-gel phase transitions, but also suggest the solubility of the biocomposites contributes the dynamics of these transitions. As the first example of enzyme-instructed solid-gel transition, this work also promises a simple, biomimetic approach to offer useful insights for the solubilisation of calcified tissues.[10]

Figure 1 shows the key molecules, steps, and results that achieve the concept in Scheme 1. The phosphopeptide (**1P**) consists of two L-amino acid residues and one D-amino acid residue (L-Phe-D-Phe-L-Tyr) in the backbone, a naphthyl group at the N-terminal, and a phosphate on the tyrosine residue. The essential design element is that, upon dephosphorylation of phosphotyrosine catalyzed by alkaline phosphatase (ALP), **1P** would turn into the corresponding hydrogelator (**1**).[11] After a facile preparation of **1P** by solid-phase peptide synthesis,[12] we dissolve **1P** in a tris-HCl buffer (pH 7.4) with an initial concentration of 0.6 wt%. The addition of $CaCl_2$ (or $SrCl_2$) results in formation of a precipitate after aging overnight. Centrifugation of the suspension separates the supernatant and precipitates. After washing the precipitates with tris-HCl buffer and lyophilisation, we obtain the powdered biocomposite made of Ca^{2+} (or Sr^{2+}) and **1P** (denoted as $Ca_x[\mathbf{1P}]_y$ or $Sr_x[\mathbf{1P}]_y$). Further analysis via atomic absorption spectroscopy shows that the ratio of calcium and **1P** in precipitate is 2:1. Since **1P** dissolves readily in phosphate-buffered saline (PBS), the increase of ionic strength (due to the addition of the alkali metal salts) is likely not responsible for the observed precipitation. Because the addition of the metal cation to the solution of **1P** directly results in precipitation, the ionic interactions between the phosphate group and Ca^{2+} (or Sr^{2+}) are responsible for the observed precipitation. Following lyophilisation, the biocomposite powder form a suspension in $Ca_3(PO_4)_2$ saturated and tris-HCl buffered water (Figure. S2). The use of saturated $Ca_3(PO_4)_2$ is necessary since it prevents the re-dissolution of the precipitates. The addition of ALP (0.25 U/mL) into the suspension of $Ca_x[\mathbf{1P}]_y$ dephosphorylates **1P** to form **1**, which self-assembles to result in supramolecular nanofibers as the matrices of the subsequently formed hydrogel. We observe

the gradual transition from suspension to a semi-transparent hydrogel after five days, agreeing with the key step illustrated in Scheme 1.

To evaluate the interactions between **1P** and metal ions, we use ^{31}P NMR spectroscopy to monitor the change in phosphate signal on the tyrosine phosphate after the addition of various amounts of the metal ions. As shown in Figure 2, when the amount of Ca^{2+} increases from 0.2 eq. to 1.0 eq., the ^{31}P signals decreases rapidly, suggesting that the concentration of phosphopeptide in the solution decreases, which is due to the formation of precipitates. This result confirms the strong interaction between **1P** and Ca^{2+}. The phosphate peak almost disappears after the addition of 2.0 eq. of calcium, indicating that a negligible amount of **1P** remains in solution. After mixing **1P** with Sr^{2+}, we observe a similar trend as with the addition of Ca^{2+}, confirming the interactions between **1P** and strontium ions. Moreover, ^{31}P NMR qualitatively indicates that the interaction of **1P** with strontium ions is slightly weaker than that of **1P** with calcium ions, as there are more soluble **1P** when the initial ratios of **1P** and the metal ions are 1:1, 2:3, and 1:2. After dispersed the powder of $Ca_x[1P]_y$ release small amounts of **1P** due to equilibrium of precipitation and dissolution, we can use ^{31}P NMR to estimate the rate of dephosphorylation of **1P**. In the suspension of $Ca_x[\mathbf{1P}]_y$, the ^{31}P signals of the tyrosine phosphate decrease significantly after the addition of ALP for 12h (Figure. S3), and completely disappear after 36h incubation, indicating that almost all **1P** in solution becomes **1**. Interestingly, the phosphate signal ($\delta = 0$) barley appears, likely due to exceptionally low solubility of calcium phosphates.[13] In the case of $Sr_x[\mathbf{1P}]_y$, ^{31}P NMR of **1P** shows the similar rapid decrease. Notably, a low intensity phosphate signal ($\delta = 0$) appears after 36h incubation, agreeing with the higher solubility of strontium phosphate than that of calcium phosphate.[13–14]

To examine the transition from the solid biocomposites to the hydrogels, we use transmission electron microscopy (TEM) to monitor the morphological changes upon the addition of various amount of ALP. After adding 0.25 U/mL ALP (upper panel of Figure. 3a), nanofibers and unstructured aggregates co-exist in the suspension of $Ca_x[\mathbf{1P}]_y$ on the first day. Though the dominant morphology appears to be unstructured aggregates, the resulting nanofibers are able to stop water flow to form a hydrogel. Meanwhile, a considerable amount of precipitates occupy the bottom of the vial (inset, Figure. 3a), indicating the initial phase separation between the precipitates and the hydrogel. In addition, energy-dispersive X-ray spectroscopy (EDX) analysis also confirms that the precipitates contain the elements of calcium ions and phosphate (Figure. S5). Notably, almost all precipitates disappear on the fifth day, and all the unstructured aggregates transform into uniform nanofibers with a width of 12 ± 2nm (Figure. 3). This result indicates that ALP converts **1P** to **1**, which self-assembles to form nanofibers, and the resulting calcium phosphate deposits in the hydrogel matrix. On the fifteenth day, TEM shows two distinct types of nanofibers coated with the aggregates: the large nanofibers with the diameters of 14–38 ± 2 nm, the short, slim nanofibers with width 6–10 ± 2 nm. The appearance of thinner nanofibers indicates the re-organization of peptides, which may be associated with the dissociation of the calcium ions from the carboxylate of the peptides. Moreover, there are nanoparticles (14–46 nm) adhering to the bigger nanofibers, and the turbidity of the hydrogel slightly and evenly increase from the 5th to 15th day (Figure. S6). This transition

from uniform nanofibers to multiple morphologies is similar with the heterogeneous nature of bone. The reappearance of large nanoparticles over time is likely associated with "Ostwald-ripening".[15] The formation of more ordered structures over time suggests an annealing process, which may be related with the arrangement of C-terminal carboxylate during the self-assembly in the hydrogel. The addition of 0.05 U/mL ALP results in different kinetics of morphological/phase transition, evidenced by much less hydrogel formation on the fifth day. TEM images of the samples on the fifth day reveal the existence of more particulate precipitates. After 15 days incubation, considerable amounts of unstructured aggregates still adhere to the nanofibers. This situation is similar to the case of hypophosphatasia that low enzyme activity results in less ordered structures. Such difference indicates that the rate of dephosphorylation—and subsequently differences in the interactions between **1P** and **1** with the calcium cations—plays an important role in determining the final structure of the mixture of the hydrogel and the recrystallized precipitates. These TEM results (Figure. S8) agree with the observation that increasing the enzyme concentration enhances the supramolecular order of assemblies of small molecules.[16] The above results suggest that enzyme amounts (or activities), undoubtedly, play a key role in controlling the morphological switch of the aggregates to the nanofibers via enzyme-instructed self-assembly. Although the addition of ALP to the suspension of $Sr_x[\mathbf{1P}]_y$ results in a similar transition from solid to hydrogel (Figure. S7), the rate is much faster. Notably, 0.05 U/mL ALP is able to convert the solid of $Sr_x[\mathbf{1P}]_y$ to semi-transparent hydrogel in five days (Figure. 3b), which is three time faster than the case of $Ca_x[\mathbf{1P}]_y$. Such a difference likely originates from different binding affinity of calcium and strontium with **1P** and the solubility difference[13] between calcium phosphates and strontium phosphates, as evidenced by the free phosphate signal in the ^{31}P NMR (Figure. S3). On the fifth day, 0.05 U/mL ALP converts most of the unstructured aggregates to helical nanofibers (13–18 ± 2 nm), differing with the result of $Ca_x[\mathbf{1P}]_y$ where unstructured aggregates adhere to nanofibers. While morphological transition of $Sr_x[\mathbf{1P}]_y$ in the presence of 0.25 U/mL ALP is similar with the observation of the suspension of $Ca_x[\mathbf{1P}]_y$ (Figure. S9), in which uniform nanofibers on fifth day transform to two types of nanofibers on fifteenth day, the nanoparticles on the nanofibers are larger, indicating that Ostwald-ripening reorganization of strontium phosphates is faster than in the case of calcium phosphates. This difference suggests that the dynamics of strontium phosphates may be a factor in the bone remodelling process, a controversy that remains to be resolved.[17]

Meanwhile, we use rheometry to examine the solid-gel transition after the addition of ALP (0.05 U/mL) to the suspension of $Ca_x[\mathbf{1P}]_y$ or $Sr_x[\mathbf{1P}]_y$. During first 40 min of the initiation stage, storage modulus (G′) and loss modulus (G″) of the suspension of $Ca_x[\mathbf{1P}]_y$ is almost constant, indicating that a low concentration of **1** has little influence on viscoelasticity of the sample. Notably, G′ is amost ten-fold higher than G″, likely resulting from the large amount of precipates in the sample. Then, G′ and G″ start to increase, and the ratio of G′/G″ is about 2.2 at 58 min, which represents the gelation point. Furthermore, the resulting stable hydrogel has G′ value of 6.8 KPa, almost 1000 times of that of the hydrogel made by **1** (7 Pa) only,[11] suggesting that the inclusion of calcium ion in the hydrogels enhances rheological properties of the hydrogels. In the case of $Sr_x[\mathbf{1P}]_y$, which results from small amount of precipitates, G″ dominates G′ during the first 20 min, suggesting that the sample behaves as

a viscous liquid. This result also implies that large amount of precipitates might lead to large ratio of G′ to G″. After 20 min, G′ starts to dominate G″, behaving as a viscoelastic material. The gelation time (20 min.) is much shorter than that of $Ca_x[\mathbf{1P}]_y$, agreeing with the weak interaction between **1P** and strontium ions which provides more unbound **1P** available for dephosphorylation and subsequent self-assembly and hydrogelation. In addition, G′ values of both the hydrogels are frequency indepenedent (0.1 rad/s to 200 rad/s), suggesting that the matrices of the hydrogels have good torelance to external force (Figure. S10).

To further examine the morphological transition regulated by ALP, we use scanning electron microscopy (SEM) to evaluate the morphological changes of $Ca_x[\mathbf{1P}]_y$ catalysed by ALP (0.25 U/mL). As shown in Figure. S11, on the first day, larger spherical aggregates dominate the plate-like structures, confirming the existence of large amounts of precipitated biocomposites. Interestingly, small spherical nanoparticles (around 80 nm) connect with each other to form large aggregates with lengths of several microns. At the fifteen days, most of spherical aggregates transform to a plate-like morphology. Together, TEM and SEM images provide a comprehensive details on the microstructures of the precipitates. The enzyme-regulated in-situ deposition of the resulting calcium phosphate likely contributes to the formation of smooth plates. Meanwhile, some spherical aggregates connect the plates, significantly enhancing the elasticity of the resulting hybrid hydrogels, further confirming the unique advantage of enzymatic transformation.

Moreover, we also test solid-gel transition of biocomposites containing **2P** (Figure. S12) that is an enantiomer of **1P. 2P** forms precipitate after binding with calcium and gradual transform to a hydrogel in the presence of ALP (0.25 U/mL) (Figure. S13). Based on natural occurring events like bone remodelling, enzyme-associated solid-gel transition of a biocomposite could be considered as a general process. Since the structural biology of bone formation[18] also confirms that the structure of peptides is another important factor, our future study will also explore the role of the structures of the phosphopeptides in the enzyme-instructed solid-gel transition.

In conclusion, we use an enzymatic reaction to shift the equilibrium of a solid substance dissolving in an aqueous solution, and to achieve a biomimetic solid-gel transition. This work not only provides a new method to prepare biological active soft materials, but also offers a useful way to control slow release of other bioactive agents, for example strontium ions[19] by allowing elaborated release profiles for enhancing bond strength.[20] Furthermore, such endogenous enzyme-instructed soft materials not only can serve as calcium phosphate source,[17b] but also provide favourable environment at interface of bone.[21] Such features might offer some unexpected beneficial effect on bond regeneration and bone adaption after surgery, which warrants further exploration.

Supplementary Material

Refer to Web version on PubMed Central for supplementary material.

Acknowledgments

This work was partially supported by NIH (CA142746) and W.M Keck foundation.

References

1. a) Golub EE, Boesze-Battaglia K. Curr Opin Orthop. 2007; 18:444–448.b) Addison WN, Azari F, Sorensen ES, Kaartinen MT, McKee MD. J Biol Chem. 2007; 282:15872–15883. [PubMed: 17383965]
2. Sapir-Koren R, Livshits G. IBMS BoneKEy. 2011; 8:286–300.
3. Hessle L, Johnson KA, Anderson HC, Narisawa S, Sali A, Goding JW, Terkeltaub R, Millan JL. Proc Natl Acad Sci U S A. 2002; 99:9445–9449. [PubMed: 12082181]
4. a) Schneider JP, Pochan DJ, Ozbas B, Rajagopal K, Pakstis L, Kretsinger J. J Am Chem Soc. 2002; 124:15030–15037. [PubMed: 12475347] b) Zhang XL, Chu XL, Wang L, Wang HM, Liang GL, Zhang JX, Long JF, Yang ZM. Angew Chem Int Edit. 2012; 51:4388–4392.c) Micklitsch CM, Knerr PJ, Branco MC, Nagarkar R, Pochan DJ, Schneider JP. Angew Chem Int Edit. 2011; 50:1577–1579.d) Cui H, Cheetham AG, Pashuck ET, Stupp SI. J Am Chem Soc. 2014; 136:12461–12468. [PubMed: 25144245]
5. a) Schnepp ZAC, Gonzalez-McQuire R, Mann S. Adv Mater. 2006; 18:1869–1872.b) Kuang Y, Shi J, Li J, Yuan D, Alberti KA, Xu Q, Xu B. Angew Chem Int Ed. 2014; 53:8104–8107.c) Gao Y, Shi J, Yuan D, Xu B. Nat Commun. 2012; 3:1033. [PubMed: 22929790] d) Yang Z, Liang G, Guo Z, Guo Z, Xu B. Angew Chem Int Ed. 2007; 46:8216–8219.e) Spoerke ED, Anthony SG, Stupp SI. Adv Mater. 2009; 21:425–430. [PubMed: 22068437]
6. a) Toledano S, Williams RJ, Jayawarna V, Ulijn RV. J Am Chem Soc. 2006; 128:1070–1071. [PubMed: 16433511] b) Debnath S, Roy S, Ulijn RV. J Am Chem Soc. 2013; 135:16789–16792. [PubMed: 24147566]
7. Gelb BD, Shi GP, Chapman HA, Desnick RJ. Science. 1996; 273:1236–1238. [PubMed: 8703060]
8. Smith L, Jennings RB, Garvin PJ, Gesler RM. Nature. 1963; 198:1311–1312. [PubMed: 13989503]
9. a) Boekhoven J, Brizard AM, van Rijn P, Stuart MCA, Eelkema R, van Esch JH. Angew Chem Int Ed. 2011; 50:12285–12289.b) Boekhoven J, Brizard AM, Kowlgi KNK, Koper GJM, Eelkema R, van Esch JH. Angew Chem Int Ed. 2010; 49:4825–4828.
10. Oliva F, Via AG, Maffulli N. BMC Med. 2012; 10
11. Shi J, Du X, Yuan D, Zhou J, Zhou N, Huang Y, Xu B. Biomacromolecules. 2014; 15:3559–3568. [PubMed: 25230147]
12. Chan, WC.; white, PD. Oxford University Press Inc; New York: 2000.
13. Haynes, WM. 96. Taylor and Francis Group, LLC; 2015.
14. Christoffersen J, Christoffersen MR, Kolthoff N, Bärenholdt O. Bone. 1997; 20:47–54. [PubMed: 8988347]
15. Voorhees PW. J Stat Phys. 1985; 38:231–252.
16. Hirst AR, Roy S, Arora M, Das AK, Hodson N, Murray P, Marshall S, Javid N, Sefcik J, Boekhoven J, van Esch JH, Santabarbara S, Hunt NT, Ulijn RV. Nat Chem. 2010; 2:1089–1094. [PubMed: 21107375]
17. a) Xie H, Ye Q. Osteoporos Int. 2015; 26:2213–2214. [PubMed: 25874352] b) Ni GX, Lin JH, Chiu PKY, Li ZY, Lu WW. J Mater Sci-mater M. 2010; 21:2897–2897.c) Cheung KMC, Lu WW, Luk KDK, Wong CT, Chan D, Shen JX, Qiu GX, Zheng ZM, Li CH, Liu SL, Chan WK, Leong JCY. Spine. 2005; 30:S84–S91. [PubMed: 16138071]
18. Weiner S, Sagi I, Addadi L. Science. 2005; 309:1027–1028. [PubMed: 16099970]
19. Tadier S, Bareille R, Siadous R, Marsan O, Charvillat C, Cazalbou S, Amedee J, Rey C, Combes C. J Biomed Mater Res B Appl Biomater. 2012; 100:378–390. [PubMed: 22102621]
20. Munch E, Launey ME, Alsem DH, Saiz E, Tomsia AP, Ritchie RO. Science. 2008; 322:1516–1520. [PubMed: 19056979]
21. Neffe AT, Pierce BF, Tronci G, Ma N, Pittermann E, Gebauer T, Frank O, Schossig M, Xu X, Willie BM, Forner M, Ellinghaus A, Lienau J, Duda GN, Lendlein A. Adv Mater. 2015; 27:1738–1744. [PubMed: 25601165]

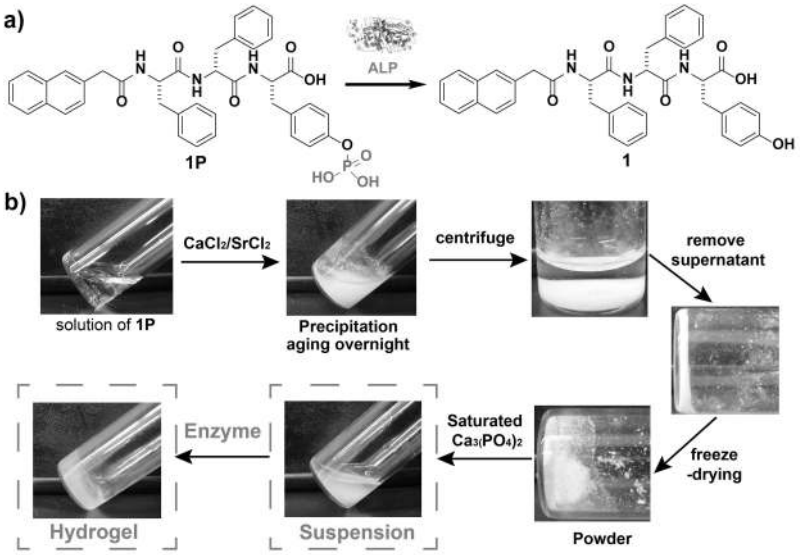

Figure 1.

a) Enzymatic dephosphorylation of **1P** to **1**. b) A typical procedure for preparation of the hydrogels via the enzymatic solid-gel transition: **1P** dissolves in 7.4 tris-HCl buffer at initial concentration of 0.6 wt% (8.29 mM), the concentration of saturated $Ca_3(PO_4)_2$ is around 3.87 μM, and $[\mathbf{1P}]_0$:$[\mathbf{M}]_0$ is 1:2.

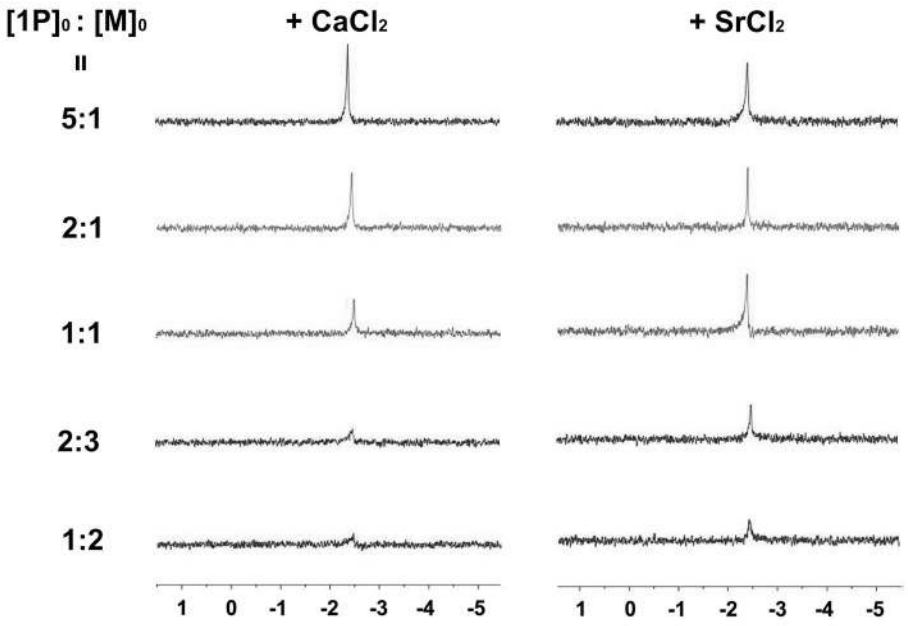

Figure 2.

^{31}P NMR spectra show the formation of precipitates made of **1P** and M^{2+} (M = Ca or Sr) after the addition of various amounts of $CaCl_2$ (left panel) and $SrCl_2$ (right panel) into the solution of **1P** (0.6 wt%) for 12h. **1P** is dissolved in pH 7.4 Tris-HCl buffer, all NMR experiment are performed at same condition (nt = 350, bs = 2).

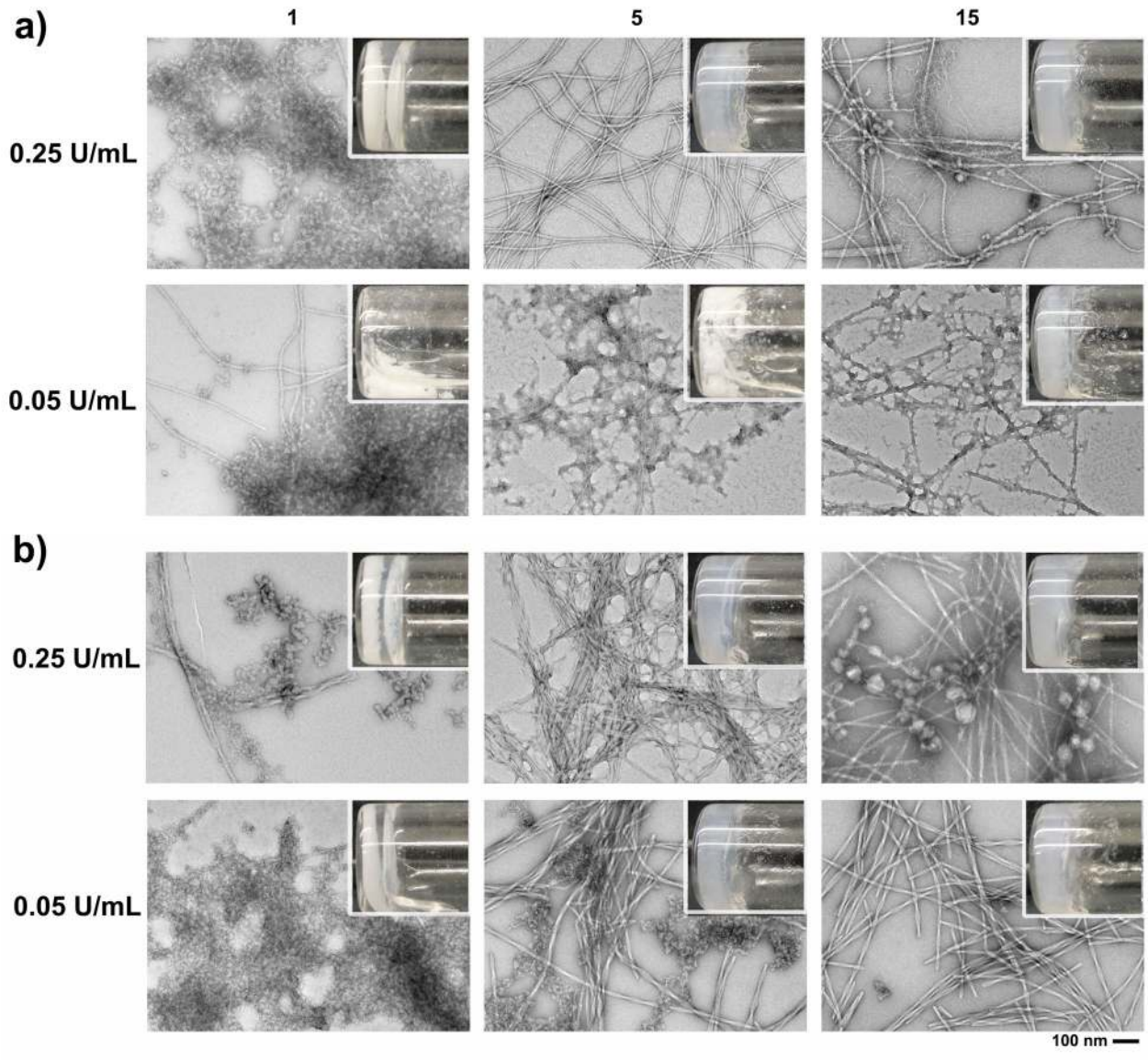

Figure 3.

TEM images showing the time course of nanostructure formation in the suspension of a) $Ca_x[\mathbf{1P}]_y$ and b) $Sr_x[\mathbf{1P}]_y$ with different amounts of ALP. $[\mathbf{1P}]_0$ = 0.6 wt%, $[\mathbf{1P}]_0$:[$Ca^{2+}]_0$ = 1:2.

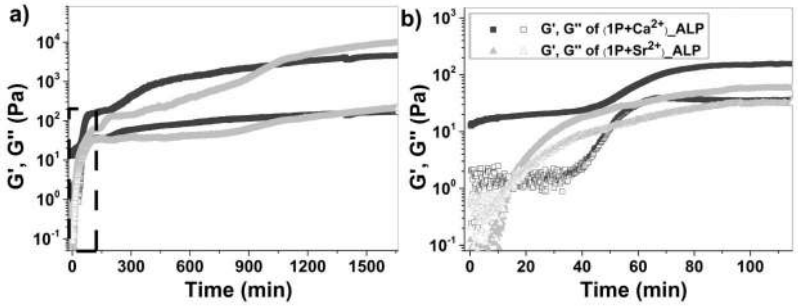

Figure 4.

a) Dynamic oscillatory rheology demonstrates the formation of a hydrogel after treating the suspension of $Ca_x[\mathbf{1P}]_y$ or $Sr_x[\mathbf{1P}]_y$ with ALP (0.05U/mL). b) Expansion of dashed box shows gelation process during the initial stage. $[\mathbf{1P}]_0$ = 0.6 wt%, $[\mathbf{1P}]_0$:$[\mathbf{M}]_0$ = 1:2.

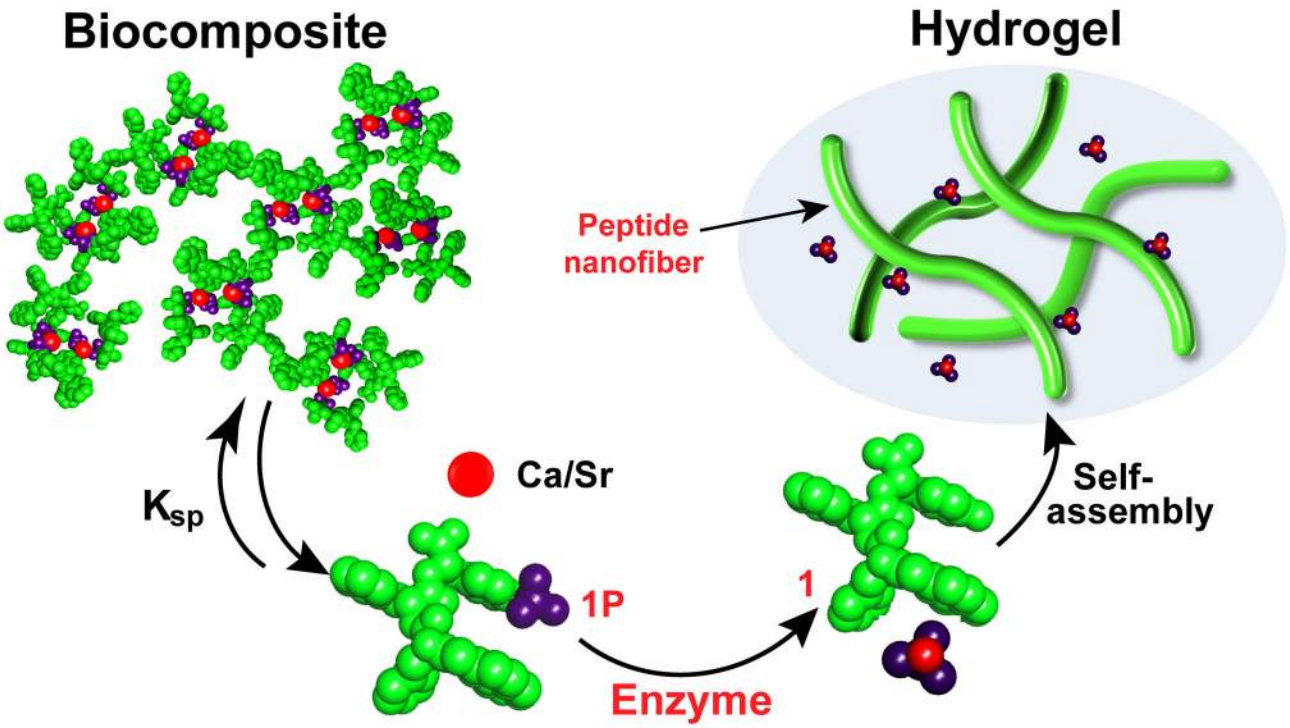

Scheme 1.

Conceptual illustration of enzyme-instructed solid-gel transition of the biocomposite made of small phosphopeptides and alkaline earth metal ions.